This is a peer-reviewed, author's accepted manuscript of the following conference output:
Timmers, V., Egea-Álvarez, A., Gkountaras, A., & Xu, L. (Accepted/In press).
Review and comparison of single and dual active bridge converters for MVDC-connected wind turbines.
Paper presented at 21st Wind & Solar Integration Workshop, The Hague, Netherlands.

REVIEW AND COMPARISON OF SINGLE AND DUAL ACTIVE BRIDGE CONVERTERS FOR MVDC-CONNECTED WIND TURBINES

Victor Timmers[1]* , Agustí Egea-Àlvarez[1], Aris Gkountaras[2], Lie Xu[1]

[1]Department of Electronic and Electrical Engineering, University of Strathclyde, Glasgow, UK
[2]Siemens Gamesa Renewable Energy, Hamburg, Germany
**E-mail: victor.timmers@strath.ac.uk*

Keywords: WIND ENERGY, CONVERTER, MVDC, SAB, DAB

Abstract

A key component for all-DC wind farms is the DC/DC converter. The converter must have multi-megawatt power capability, a high step-up ratio, provide galvanic isolation, and operate efficiently while being able to fit in the wind turbine nacelle. The single active bridge (SAB) and dual active bridge (DAB) converters in standalone or cascaded configuration are promising topologies that have the potential to meet these requirements. This paper reviews the operation and control of these converters, and compares their volume, weight, and efficiency for a 15 MW wind turbine with 80 kV DC connection. The results show that the standalone topologies are significantly smaller and lighter than their cascaded counterparts. However, all topologies fit inside the wind turbine nacelle. The SAB designs are the most efficient and robust, as they use diodes in the output bridge. The DAB topologies have the advantage of bidirectional power flow at the cost of additional switches and losses. The standalone DAB requires series-connected switches in the output bridge, which may difficult to implement. The cascaded topologies offer higher reliability without significantly increasing losses, making them the most attractive option for future DC wind turbines.

1 Introduction

Traditionally, offshore wind power plants have used medium voltage AC (MVAC) collection systems with either high voltage AC (HVAC) or high voltage DC (HVDC) export systems. As the offshore wind industry has matured, the size and distance from shore of offshore wind farms has continually increased. This, together with the continual development of power semiconductors, has generated significant interest in using medium voltage DC (MVDC) in the collection system instead, resulting in an all-DC wind farm. This has the potential to provide cost savings when connecting to HVDC or even directly to shore [1].

One of the main components required for these all-DC wind farms is a high-power, high-step up DC/DC converter. This interfaces the low voltage wind turbine generator with the MVDC collection network, as shown in Fig. 1. Depending on the wind power plant design, string-level or farm-level DC/DC converters can also be used to further increase the voltage for the transmission stage [2, 3]. The focus of this paper will be on the wind turbine converter.

A multitude of converter topologies has been put forward for high power DC/DC conversion, which can broadly be categorised into isolated and non-isolated designs, resonant and non-resonant designs, modular and non-modular designs [4]. It is therefore necessary to perform a downselection of DC/DC converter topologies to determine the appropriate design for use in DC wind turbines.

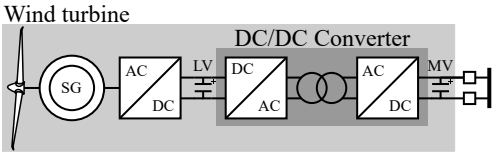

Fig. 1: DC/DC converter location in MVDC-connected wind turbine

Previous research [5] has shown that cost-effective all-DC wind farms require a DC/DC converter with high power handling capability of 15 MW to accommodate the rating of future wind turbines. The converter needs to have a high voltage step-up ratio. Wind turbine generators are typically rated at a voltage of 690 V to a few kV [6], whereas a DC collection system will need to be able to achieve voltages of 80 kV or more [5]. In all cases, the converter must have acceptable dimensions and weight to be able to be located inside the nacelle or wind turbine tower. For safety considerations, and to enable high-step up ratios, galvanic isolation is necessary [7, 8].

Beyond these functional requirements, the ideal converter topology will have a high reliability, due to the difficulty accessing and repairing offshore wind turbines. Further performance requirements include a high efficiency at wide operating range and a low component number and cost.

Based on these requirements, non-isolated converters, such as those presented in [9, 10], are not considered due to safety issues. Resonant converters, which use a separate resonant tank consisting of a combination of inductors and capacitors, aim

to reduce switching losses by switching at zero current and/or zero voltage [3]. The efficiency benefits over non-resonant designs are not guaranteed, however [3, 7, 11]. The additional complexity of resonant designs also makes them unlikely candidates for DC wind turbines in the near future. These were therefore not selected for further investigation.

The remaining converter topologies include isolated, non-resonant converters which can be modular or non-modular. Of these, studies have shown that both the single active bridge (SAB) [12, 13] and dual active bridge (DAB) [14, 15] are promising topologies for DC wind turbines. However, there is a lack of research on how these converters compare for this application. Important questions remain on what impact the modular vs. non-modular design choice has, and how the topology choice affects the transformer size and ability to fit in the nacelle, as well as the overall converter efficiency.

This paper fills this gap by first reviewing the SAB and DAB converters in terms of their components, operation and control when used in DC wind turbines. The options for connecting multiple converters together in a cascaded arrangement are then discussed. The design methodology and loss calculation of the medium frequency transformer is presented. Finally, the standalone and cascaded versions of the SAB and DAB are compared in terms of their volume, weight and efficiency.

2 Single active bridge converter

2.1 Schematic

The SAB converter schematic is shown in Fig. 2a. The SAB consists of an active full bridge inverter at the primary side and a passive full bridge rectifier on the secondary. The bridges are connected through a medium frequency transformer (MFT) with a leakage inductance used for the power transfer. The switches on the primary side include a transistor, typically an IGBT, an anti-parallel diode and potentially a soft-switching capacitor connected in parallel, depending on the design. The voltage is filtered by a capacitor at both the input and output of the converter.

2.2 Operation

The SAB creates a square wave voltage by switching transistor pairs S_1,S_4 and S_2,S_3. The duty cycle determines the duration of the ON state for S_3 and S_4, thereby controlling the width of the voltage pulse and the power transfer from the input to output bridge.

The SAB can be operated in either continuous current mode (CCM) or discontinuous current mode (DCM), depending on the leakage inductance, duty cycle and voltage. In CCM, the converter can achieve soft-switching through the use of capacitors connected in parallel to the switches, but at lower output powers the converter loses this soft-switching capability as it operates in DCM. This is described in more detail in [16]. In this case, the switch capacitors increase the turn-off losses of the converter at low power output [13, 17].

For large wind turbine applications, which do not operate at full power continuously, the SAB is therefore typically designed to operate exclusively in DCM, without the use of soft-switching capacitors. This simplifies the design and reduces the filter inductance requirements [13, 18], at the cost of higher current stresses [7]. The waveforms for the SAB operating in DCM are shown in Fig. 2b.

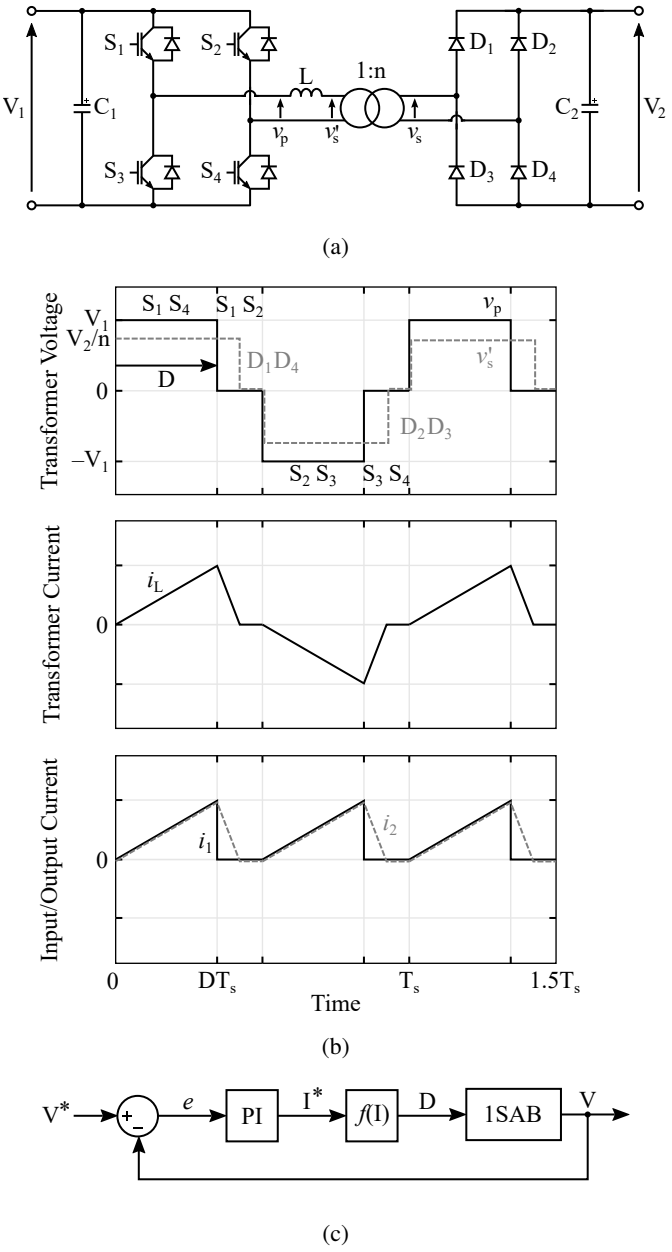

Fig. 2: The single active bridge converter (SAB), (a) schematic, (b) waveforms, (c) control

Based on the waveforms, the following equations can be derived describing the steady-state operation. When switch S_1 and S_4 are ON, the rise in current in the transformer inductance is given by

$$\Delta i_{L_{ON}} = \frac{V_1 - V_2/n}{fL} D \tag{1}$$

where V_1 is the DC input voltage, V_2 is the DC output voltage, n is the transformer turns ratio, L is the transformer leakage inductance, D is the duty cycle and f is the switching frequency.

When switch S_4 turns off, the diodes D_1 and D_4 continue conducting until the current has returned to zero. In this interval, the fall in current is given by

$$\Delta i_{L_{OFF}} = -\frac{V_2/n}{fL} D_f \tag{2}$$

Where D_f is the fall duration of the inductor current. The rise and fall in current in the transformer leakage inductance must be equal, resulting in a fall duration of

$$D_f = \left(\frac{nV_1}{V_2} - 1\right) D \tag{3}$$

To maintain discontinuous mode operation, the total rise and fall time may not exceed one half of the switching cycle, resulting in a maximum duty cycle, D_{max}, of

$$D_{max} = \frac{V_2}{2nV_1} \tag{4}$$

The average output power is given by

$$P_2 = \frac{V_1}{fL}\left(V_1 - \frac{V_2}{n}\right) D^2 \tag{5}$$

The maximum power output is achieved at a duty cycle of D_{max}. The average output and input currents can be calculated using standard equations

$$I_2 = P_2/V_2 \quad ; \quad I_1 = nI_2 \tag{6}$$

2.3 Control

The basic control structure of the SAB is shown in Fig. 2c. The controller can be designed to either control the input or the output voltage. It consists of a proportional-integral controller which sets the desired current based on the voltage error using the transfer function

$$PI(s) = K_p + \frac{K_i}{s} \tag{7}$$

The gains K_p and K_i can be tuned manually or calculated using techniques such as the symmetrical optimum method [18]. The resulting current setpoint is converted to a duty cycle for the converter switches, by rearranging (5) and (6) for the duty cycle D, resulting in

$$D = \sqrt{\frac{fL}{V_1 - \frac{V_2}{n}}} \sqrt{I_1} \tag{8}$$

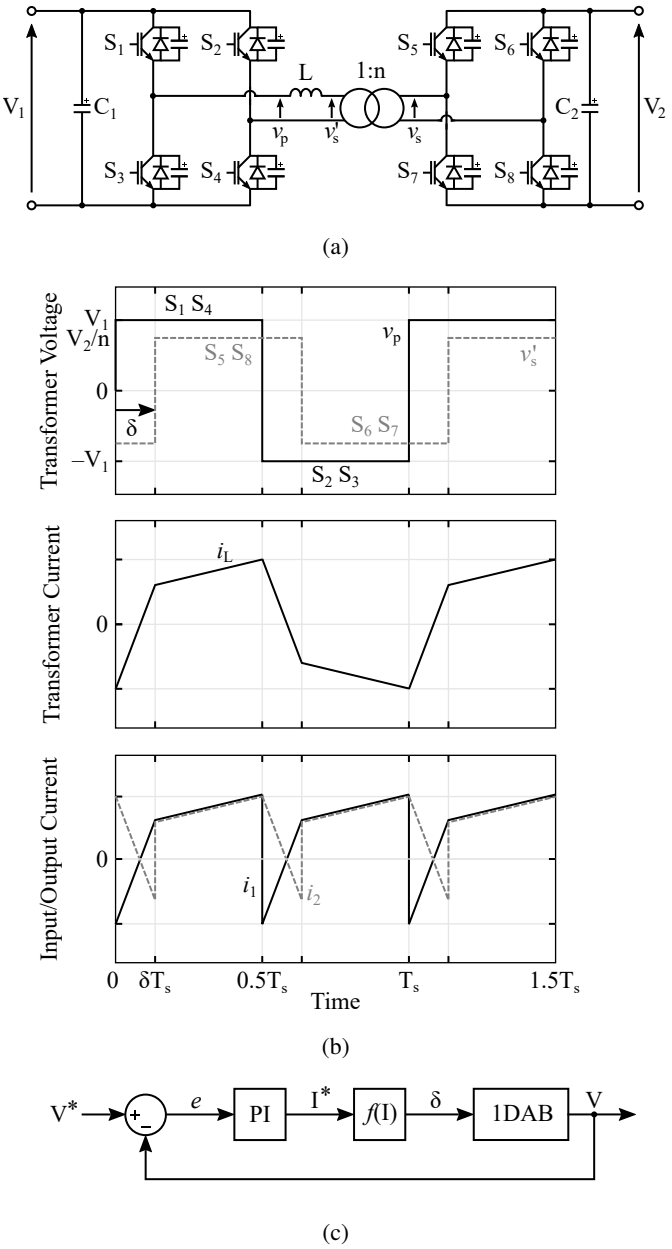

Fig. 3: The dual active bridge converter (DAB), (a) schematic, (b) waveforms, (c) control

3 Dual active bridge converter

3.1 Schematic

The DAB converter schematic is shown in Fig. 3a. The DAB has a similar topology to the SAB, with the main difference being an active bridge on the secondary. This allows bidirectional power flow. As with the SAB, the DAB transformer's leakage inductance can be used for the power transfer, resulting in a more compact overall design.

3.2 Operation

The DAB creates a square wave voltage on both bridges which are shifted by a phase angle, δ. The phase angle determines the direction of power exchange, with power flowing from the leading to lagging bridge. Both pairs of switches on each bridge have a fixed duty cycle of one half of the switching period. The DAB operates exclusively in CCM, with soft-switching achieved through the use of capacitors connected in parallel with each switch [17].

The voltage and current waveforms of the DAB are shown in Fig. 3b. The inductor current is symmetrical over half the period. During the first interval, when switches S_1 and S_4 are ON but S_5 and S_8 are still OFF, the rise in inductor current is given by

$$\Delta i_{L_1} = \frac{V_1 + V_2/n}{fL}\delta \tag{9}$$

During the second interval, switches S_5 and S_8 are turned ON and the current increases by

$$\Delta i_{L_2} = \frac{V_1 - V_2/n}{fL}\Big(\frac{1}{2} - \delta\Big) \tag{10}$$

For soft-switching to occur, the current i_L must be negative at the start of the period and positive at the start of the second half of the period. The minimum angle to attain soft-switching is dependent on the voltage conversion ratio [17], calculated using

$$\delta_{min} = \frac{1}{4}\Big(1 - \frac{V_2}{nV_1}\Big) \tag{11}$$

Hence, when the voltage conversion ratio is unity, soft-switching can be achieved over the full operating range.

The average power output of the DAB can be calculated using the equation

$$P_2 = \frac{V_1 V_2}{fLn}\delta(1 - 2\delta) \tag{12}$$

The maximum power output is achieved at a phase shift of 0.25. The corresponding input and output currents can be calculated using the standard equations (6).

3.3 Control

The basic control structure of the DAB is shown in Fig. 3c. Similar to the SAB, the controller can be designed to either control the input or the output voltage and uses a PI controller to set the desired output current. This is converted to a phase angle shift by rearranging (12) for the phase shift δ, resulting in

$$\delta = \frac{1}{4}\Big(1 - \sqrt{1 - \frac{8fLI_2n}{V_1}}\Big) \tag{13}$$

More sophisticated control schemes have been proposed and implemented for the DAB to reduce its large circulating reactive current [19], which occurs when the voltage conversion ratio is not equal to one. However, since the input and output voltage of the converter do not vary significantly in DC wind turbines applications, simple phase shift control can be used.

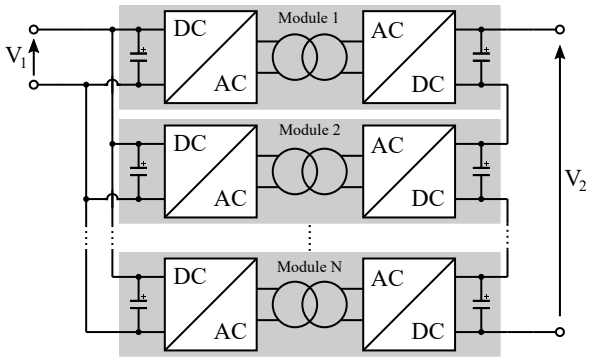

Fig. 4: Schematic of an input-parallel, output-series cascaded DC/DC converter

4 Cascaded converters

Due to the high power and high voltage requirements for the converter, several papers have proposed cascaded SAB (CSAB) or cascaded DAB (CDAB) converters, where individual converters are connected together [20, 21]. Despite the wide application of multilevel modular converters (MMCs) in HVDC applications, for high power DC/DC conversion, a cascaded connection of the converters is typically more efficient and cost-effective [15].

There are four standard cascaded connection topologies, including input-series output-series (ISOS), input-series output-parallel (ISOP), input-parallel output-parallel (IPOP), and input-parallel output-series (IPOS) [6]. The series connection allows the voltage to be increased, whereas a parallel connection allows for current sharing between the converters. This means that for the high-power, high voltage step-up requirements of a DC wind turbine, the IPOS connection is most suitable. This topology is illustrated in Fig. 4.

The number of converter modules will depend on the design goals of the converter. One approach is to have a 1:1 turns ratio for the MFT transformer [22]. This has the benefit of simplifying the transformer design and, for the DAB, allows the voltage conversion ratio to stay close to unity, reducing circulating currents. However, if the voltage of the secondary is much higher than the primary, a large number of modules will be required.

An alternative approach is to select the number of modules based on the blocking voltage and current rating of the selected semiconductors [23]. This means the series-connection of switches, which may be difficult to implement, is avoided. Additional redundant modules can also be added to increase the reliability and fault-tolerance of the converter [20].

Further benefits of a cascaded configuration include the ability to use an outer control loop to balance the power between non-identical modules and the use of interleaved switching, where the switching instants of the modules are phase-shifted to reduce the overall ripple without increasing losses [18].

Table 1 Material properties for the MFT [23, 25]

Symbol	Property	Unit	Value
B_{sat}	Core magnetic saturation	T	1.17
ρ_c	Core density	kg/m^3	7330
k_c	Core fill factor		0.75
k	First Steinmetz constant	W/m^3	0.036
α	Second Steinmetz constant		1.64
β	Third Steinmetz constant		2.10
E_{max}	Max. insulation strength	kV/mm	29
ρ_{ins}	Insulation density	kg/m^3	500

5 Medium Frequency Transformer

5.1 Design

The MFT is an essential component of the isolated DC/DC converter. Research has found a frequency of 1 kHz results in a large size and weight reduction of the transformer without excessive additional losses compared to a 50 Hz transformer [24]. Due to the high power requirements, non-standard frequency and the importance of the leakage inductance, an off-the-shelf transformer cannot be used in the wind turbine DC/DC converter. Instead, the MFT must be specifically designed for this application.

The transformer design procedure is based on that set out in [25] and [26]. The transformer is a shell type with the low and high voltage windings concentrically wound around the central limb. The procedure starts with the specification of fixed design parameters, such as nominal power, input and output voltages and frequency. In addition, the core and insulation materials are selected. These are shown in Table 1. The transformer core is assumed to use copper foil in the primary winding and litz wires in the secondary winding.

Once the fixed parameters are set, there are a series of free parameters which can be varied to obtain an optimal design. These include the number of parallel layers in the primary and secondary windings, the number of turns per layer in the primary, the number of core stacks, and the current density of the primary and secondary windings. This results in a wide range of possible transformer designs, which are each evaluated in terms of volume, weight and losses.

5.2 Losses

The transformer losses considered include the copper winding losses and the iron core losses. The DC winding resistance for each winding is calculated using

$$R_{dc} = \frac{\rho_{Cu} N MLT}{A_{Cu}} \tag{14}$$

To calculate the ratio of AC to DC resistance at a given frequency, the following equations are used [26]

$$K_{ac} = \frac{1}{2} y M_y + (2m-1)^2 D_y \tag{15}$$

Table 2 Fixed parameters for the DC/DC converter comparison

Parameter	SAB	DAB	CSAB	CDAB
Number of modules N	1	1	12	18
Module power P_n (MW)	15	15	1.25	0.83
Output voltage V_2 (kV)	80	80	80	80
Turns ratio n	78	67	6.67	3.75
Inductance L (μH)	2.55	4.99	30.6	94.8

where

$$y = \frac{w}{\delta} \quad ; \quad \delta = \frac{0.071}{\sqrt{f_h}} \tag{16}$$

$$M_y = \frac{\sinh(y) + \sin(y)}{\cosh(y) - \cos(y)} \tag{17}$$

$$D_y = \frac{\sinh(y) - \sin(y)}{\cosh(y) + \cos(y)} \tag{18}$$

The copper winding losses can then be calculated by decomposing the transformer current in its harmonic components and summing the resulting loss

$$P_{Cu} = \sum_h I_h^2 K_{ac,h} R_{dc} \tag{19}$$

Where I_h is the magnitidue of the current with harmonic order h, and $K_{ac,h}$ is the ratio of AC to DC resistance at the frequency of harmonic order h.

To calculate the iron core losses per unit volume, the Improved Generalised Steinmetz Equation (IGSE) is used. This is defined as [27]

$$P_{core} = \frac{1}{T} \int_0^T k_i \left| \frac{dB}{dt} \right|^\alpha (\Delta B)^{\beta-\alpha} dt \tag{20}$$

where B is the instantaneous magnetic flux density, ΔB is the peak-to-peak magnetic flux density, and k_i is calculated using

$$k_i = \frac{k}{(2\pi)^{\alpha-1} \int_0^{2\pi} |\cos\theta|^\alpha \, 2^{\beta-\alpha} d\theta} \tag{21}$$

where k, α, and β are the Steinmetz parameters of the iron core material. For a square wave excitation voltage with duty cycle D, the core power loss becomes [28]

$$P_{core} = \frac{2D}{D^\alpha} k_i f^\alpha B_m^\beta 2^\beta V_{core} \tag{22}$$

where B_m is the maximum magnetic flux density, given by

$$B_m = \frac{V_1 D}{2 f N_1 A_{core} k_c} \tag{23}$$

6 Comparison

Four converter configurations were compared, including the standalone and cascaded versions of the SAB and DAB. The converter parameters are based on [5] and set out in Table 2.

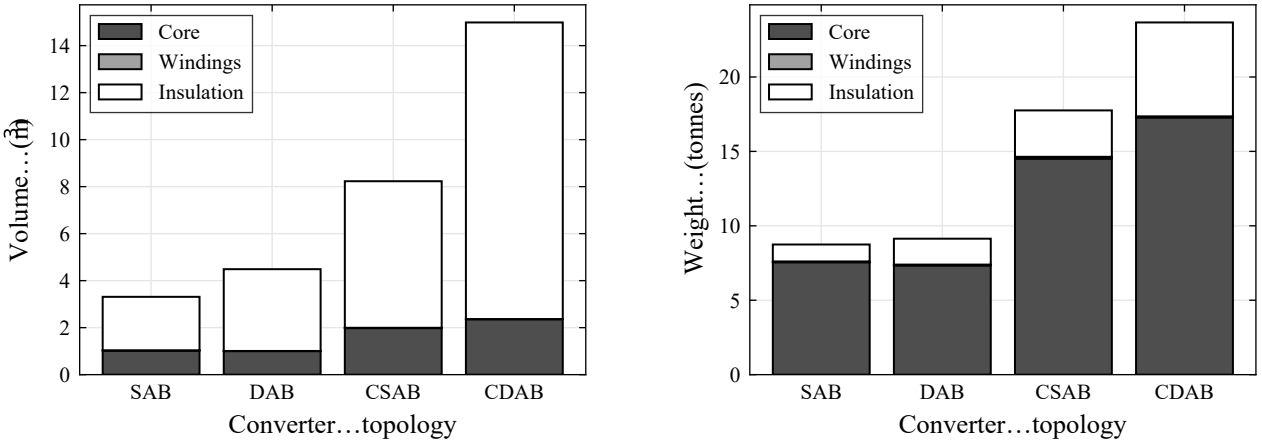

Fig. 5: Transformer comparison results, (a) volume, (b) weight

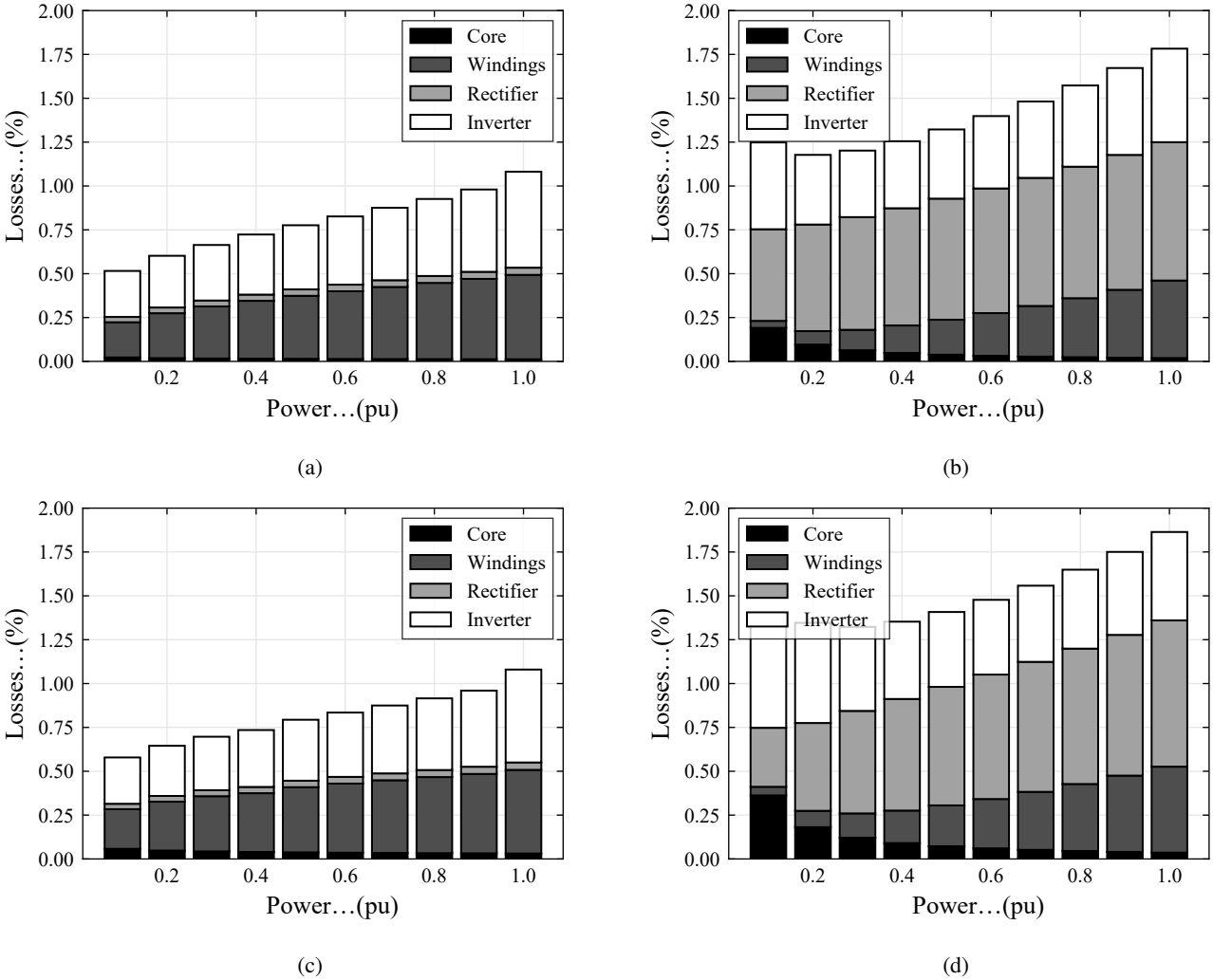

Fig. 6: Converter losses over the operating range, (a) Single active bridge, (b) Dual active bridge, (c) Cascaded single active bridge, (d) Cascaded dual active bridge

State of the art IGBT module ratings are 1.7 kV, 3.6 kA for the input bridge [29], and 6.5 kV, 250 A for the output bridge [30] in the DAB converter. For the output bridge of the SAB converter, diodes can achieve ratings of 9.0 kV, 550 A [31].

The standalone SAB and DAB require 8 IGBTs to be connected in parallel in the input bridge to be able to carry the current at maximum output power. The SAB and DAB require 12 and 18 series connected diodes and IGBTs, respectively, to withstand the output voltage. The series connection of IGBTs in particular may be practically difficult to implement due to issues with perfectly synchronising gate drives and sharing voltage equally [32].

The cascaded versions of the converters, on the other hand, are designed to not need any parallel or series connected semiconductors within each module. The CSAB and CDAB require 12 and 18 modules in IPOS configuration, respectively.

6.1 Volume and Weight

A large number of designs are possible for the MFT. Therefore, to enable a comparison, the selected designs for each converter were set to be those with the highest power density for a minimum full-load efficiency of 99.5%.

The transformer comparison results are shown in Fig. 5. The results show that for the same efficiency, the SAB transformer has a 26% smaller volume and 4% lower weight at 3.3 m^3 and 8.7 tonnes, compared to the DAB transformer's 4.5 m^3 and 9.1 tonnes.

The transformers in each module of the cascaded topologies are 14% to 20% of the volume and weight of the standalone versions. However, due to the multiple modules required, the overall volume and weight of the CSAB is more than twice that of the standalone version. For the CDAB, the volume is three times and the weight is 2.5 times that of the standalone version. Despite this, all of these converter transformers are significantly smaller and lighter than standard 50 Hz transformers and they are able to fit inside the nacelle of a 15 MW turbine.

6.2 Efficiency

The losses of the converters consist of the transformer losses, as well as the switching and conduction losses of the semiconductors. The transformer losses were calculated using the equations set out in Section 5.2. The switching and conduction losses were calculated by performing PLECS simulations using the semiconductor datasheets [29–31].

The efficiency results are shown in Fig. 6. The standalone SAB has the highest efficiency of the four studied topologies, with losses ranging from 0.5% to 1.1%, see Fig. 6a. This is due to the low losses of the diodes used in the rectifier. The standalone DAB losses, shown in Fig. 6b, range from 1.2% to 1.8%. Most of the additional losses are due to the IGBT switching losses in the rectifier. The core losses are also relatively high for lower power outputs, since the DAB operates with a constant duty cycle, and therefore constant core losses, over the entire operating range.

The losses of the CSAB and CDAB are shown in Fig. 6c and Fig. 6d, respectively. The cascaded converters have very similar losses to their standalone counterparts. Despite having a larger total number of switches in the input bridge, the primary currents are lower, resulting in only marginally higher losses at lower power outputs. The transformer core losses are also slightly higher due to the larger total transformer core volume.

Overall, all four DC/DC converter topologies manage to attain similar levels of efficiency as current direct drive wind turbine converters.

7 Conclusion

This paper has reviewed the components, operation and control of the SAB and DAB, and discussed how they can be arranged in a standalone or cascaded configuration. A comparison of the transformer volume and weight, as well as the overall converter losses was performed for a 15 MW wind turbine converter connected to a 80 kV collection system.

The analysis has shown the volume and weight of the standalone converters are lower than that of the cascaded converters. However, the relative benefits of this are limited since all topologies use transformers that fit inside the wind turbine nacelle and represent space and weight savings compared to existing low frequency transformers. In terms of efficiency, the SAB designs can achieve close to 99% efficiency over the operating range, whereas the DAB designs have an average efficiency closer to 98.5%.

Overall, for wind turbines which only require unidirectional power flow, both the SAB and CSAB are suitable. The CSAB is more attractive due to its higher reliability without suffering from a significant increase in losses. If the wind turbine requires bidirectional power flow, the CDAB is recommended. Despite its lower volume, weight and losses, the standalone DAB requires series-connected IGBTs in the output bridge which limits the practical application of this topology.

8 Acknowledgements

This work was funded by EPSRC Industrial CASE number EP/T517665/1 and Siemens Gamesa Renewable Energy.

References

[1] V. Timmers, A. Egea-Àlvarez, and A. Gkountaras, "A systematic review of DC wind farm collector cost-effectiveness," in *17th Int. Conf. on AC and DC Power Trans.*, pp. 114–119, IET, 2021.

[2] S. Coffey, V. Timmers, R. Li, G. Wu, and A. Egea-Àlvarez, "Review of MVDC applications, technologies, and future prospects," *Energies*, vol. 14, no. 24, p. 8294, 2021.

[3] L. Max and S. Lundberg, "System efficiency of a DC/DC converter-based wind farm," *Wind Energ.*, vol. 11, no. 1, pp. 109–120, 2008.

[4] J. D. Paez, D. Frey, J. Maneiro, S. Bacha, and P. Dworakowski, "Overview of DC–DC converters dedicated to HVDC grids," *IEEE Trans. Power Del.*, vol. 34,

no. 1, pp. 119–128, 2018.

[5] V. Timmers, A. Egea-Àlvarez, A. Gkountaras, R. Li, and L. Xu, "All-DC offshore wind farms: When are they more cost-effective than ac designs?," *IET Renew. Power Gener.*, 2022.

[6] Y. Lian, *DC/DC Converter for Offshore DC Collection Network*. PhD thesis, University of Strathclyde, 2016.

[7] C. Dincan, P. Kjaer, Y.-h. Chen, S.-M. Nielsen, and C. L. Bak, "Selection of DC/DC converter for offshore wind farms with MVDC power collection," in *19th Eur. Conf. on Power Electron. and Appl. (EPE'17 ECCE Europe)*, pp. P–1, IEEE, 2017.

[8] A. Follo, O. Saborío-Romano, E. Tedeschi, and N. A. Cutululis, "Challenges in all-DC offshore wind power plants," *Energies*, vol. 14, no. 19, p. 6057, 2021.

[9] W. Chen, A. Q. Huang, C. Li, G. Wang, and W. Gu, "Analysis and comparison of medium voltage high power DC/DC converters for offshore wind energy systems," *IEEE Trans. Power Electron.*, vol. 28, no. 4, pp. 2014–2023, 2012.

[10] D. Jovcic, "Step-up DC–DC converter for megawatt size applications," *IET Power Electron.*, vol. 2, no. 6, pp. 675–685, 2009.

[11] Y. Zhou, D. Macpherson, W. Blewitt, and D. Jovcic, "Comparison of DC-DC converter topologies for offshore wind-farm application," in *6th IET Int. Conf. on Power Electron., Mach. and Drives (PEMD 2012)*, pp. 1–6, IET, 2012.

[12] K. Park and Z. Chen, "Analysis and design of a parallel-connected single active bridge DC-DC converter for high-power wind farm applications," in *2013 15th Eur. Conf. Power Electron. Appl. (EPE)*, pp. 1–10, IEEE, 2013.

[13] L. Max and T. Thiringer, "Control method and snubber selection for a 5 MW wind turbine single active bridge DC/DC converter," in *2007 Eur. Conf. Power Electron. Appl.*, pp. 1–10, IEEE, 2007.

[14] R. W. De Doncker, D. M. Divan, and M. H. Kheraluwala, "A three-phase soft-switched high-power-density DC/DC converter for high-power applications," *IEEE Trans. Ind. Appl.*, vol. 27, no. 1, pp. 63–73, 1991.

[15] S. P. Engel, M. Stieneker, N. Soltau, S. Rabiee, H. Stagge, and R. W. De Doncker, "Comparison of the modular multilevel DC converter and the dual-active bridge converter for power conversion in HVDC and MVDC grids," *IEEE Trans. Power Electron.*, vol. 30, no. 1, pp. 124–137, 2014.

[16] C. Fontana, M. Forato, M. Bertoluzzo, and G. Buja, "Design characteristics of SAB and DAB converters," in *2015 Int. Aegean Conf. Elec. Mach. & Power Electron. (ACEMP)*, pp. 661–668, IEEE, 2015.

[17] C. Fontana, M. Forato, K. Kumar, M. T. Outeiro, M. Bertoluzzo, and G. Buja, "Soft-switching capabilities of SAB vs. DAB converters," in *IECON 2015-41st Annual Conf. IEEE Ind. Electron. Soc.*, pp. 003485–003490, IEEE, 2015.

[18] K. Park and Z. Chen, "Control and dynamic analysis of a parallel-connected single active bridge DC–DC converter for dc-grid wind farm application," *IET Power Electron.*, vol. 8, no. 5, pp. 665–671, 2015.

[19] B. Zhao, Q. Song, W. Liu, and Y. Sun, "Overview of dual-active-bridge isolated bidirectional DC–DC converter for high-frequency-link power-conversion system," *IEEE Trans. Power Electron.*, vol. 29, no. 8, pp. 4091–4106, 2013.

[20] Y. Lian, G. Adam, D. Holliday, and S. Finney, "Modular input-parallel output-series DC/DC converter control with fault detection and redundancy," *IET Gener., Transm. & Distrib.*, vol. 10, no. 6, pp. 1361–1369, 2016.

[21] X. Rong, J. K. Shek, and D. E. Macpherson, "The study of different unidirectional input parallel output series connected DC-DC converters for wind farm based multi-connected DC system," *Int. Trans. Elec. Energy Sys.*, vol. 31, no. 5, p. e12855, 2021.

[22] M. Kaymak, R. W. De Doncker, and T. Jimichi, "Design and verification of a medium-frequency transformer in a three-phase dual-active bridge DC-DC converter for medium-voltage grid connection of offshore wind farms," in *2020 IEEE Appl. Power Electron. Conf. (APEC)*, pp. 2694–2701, IEEE, 2020.

[23] M. Mogorovic and D. Dujic, "Sensitivity analysis of medium-frequency transformer designs for solid-state transformers," *IEEE Trans. Power Electron.*, vol. 34, no. 9, pp. 8356–8367, 2018.

[24] L. Max, *Design and Control of a DC Collection Grid for a Wind Farm*. PhD thesis, Chalmers University of Technology, 2009.

[25] M. A. Bahmani, T. Thiringer, and M. Kharezy, "Design methodology and optimization of a medium-frequency transformer for high-power DC–DC applications," *IEEE Trans. Ind. Appl.*, vol. 52, no. 5, pp. 4225–4233, 2016.

[26] L. Max, *Energy evaluation for DC/DC converters in dc-based wind farms*. Lic. thesis, Chalmers University of Technology, 2007.

[27] K. Venkatachalam, C. R. Sullivan, T. Abdallah, and H. Tacca, "Accurate prediction of ferrite core loss with nonsinusoidal waveforms using only steinmetz parameters," in *Proc. IEEE Workshop Comput. Power Electron.*, pp. 36–41, IEEE, 2002.

[28] M. Bahmani, *Design and Optimization Considerations of Medium-Frequency Power Transformers in High-Power DC-DC Applications*. PhD thesis, Chalmers University of Technology, 2016.

[29] Infineon Technologies AG, *Datasheet FZ3600-R17HP4_B2*, 2016.

[30] Infineon Technologies AG, *Datasheet FD250R65KE3-K*, 2021.

[31] Infineon Technologies AG, *Datasheet D471N*, 2014.

[32] P. R. Palmer and A. N. Githiari, "The series connection of igbts with active voltage sharing," *IEEE Trans. Power Electron.*, vol. 12, no. 4, pp. 637–644, 1997.